frontiers | Frontiers in Energy Research

TYPE Original Research
PUBLISHED 27 November 2024
DOI 10.3389/fenrg.2024.1499447



OPEN ACCESS

EDITED BY
Tunde Bello-Ochende,
University of Cape Town, South Africa

REVIEWED BY
Aggrey Mwesigye,
University of Calgary, Canada
Junjiang Bao,
Dalian University of Technology, China

*CORRESPONDENCE
Anoop Kumar Shukla,
shukla.anoophbti@gmail.com

RECEIVED 20 September 2024
ACCEPTED 25 October 2024
PUBLISHED 27 November 2024

CITATION
Sharma A, Shukla AK, Singh O and Sharma M (2024) Techno-economic assessment of a solar-based novel power generation system formed from a helium Brayton cycle and an organic Rankine flash cycle.
*Front. Energy Res.* 12:1499447.
doi: 10.3389/fenrg.2024.1499447



# Techno-economic assessment of a solar-based novel power generation system formed from a helium Brayton cycle and an organic Rankine flash cycle

Achintya Sharma[1], Anoop Kumar Shukla[1]*, Onkar Singh[2,3] and Meeta Sharma[1]

[1]Department of Mechanical Engineering, Amity University, Noida, India, [2]Department of Mechanical Engineering, Harcourt Butler Technical University, Kanpur, India, [3]Veer Madho Singh Bhandari Uttarakhand Technical University, Dehradun, India

The essential element of human existence is energy. However, conventional energy sources are steadily running out, and it is necessary to create an energy-efficient renewable power generation system. In the present work, an organic Rankine flash cycle (ORFC) was implemented in a conventional solar power tower (SPT)-helium Brayton cycle (HBC) to generate extra power, enhancing efficiency. The performance of the proposed SPT-based power generation system (SPT-HBC-ORFC) was analyzed based on thermodynamic and economic aspects using computational techniques through engineering equation solver software. The results revealed that the proposed power plant's energy efficiency, exergy efficiency, power output, and total cost rate were 33.68%, 33.70%, 33.69%, and 15.47%, respectively, higher than those of a conventional SPT-HBC system at the given conditions. With 39% of all exergy destruction, heliostats are the source of the greatest exergy destruction. Parametric analysis reveals that solar subsection parameters had a larger effect on the performance of the proposed power plant. Comparisons with previous studies show that the present power generation system is more efficient than the SPT-based supercritical $CO_2$ Brayton and Rankine cycles.

KEYWORDS

**solar power tower, renewable energy sources, organic Rankine flash cycle, combined cycle, helium Brayton cycle**

## 1 Introduction

Energy is the prime factor for living. Energy demand is increasing due to population growth and industrial development. However, the source of energy is continuously being depleted. Therefore, to provide a continuous energy supply, it is necessary to create alternative energy sources. In this regard, solar energy is one of the best options for providing clean and long-lasting energy (Bataineh, 2024). Concentrating solar power (CSP) and photovoltaic (PV) technologies are two dominant methods of harnessing solar energy, each with distinct advantages. Although PV has garnered widespread adoption due to its lower costs and ease of installation, CSP offers unique long-term benefits that position it as a critical complement and, in some cases, a superior alternative to

PV, particularly in large-scale power generation (Alami et al., 2023). Unlike PV systems, which convert sunlight directly into electricity, CSP harnesses the sun's heat to drive steam turbines, allowing integration with thermal energy storage systems. This capability is crucial because it provides reliable power generation even when the sun is not shining, addressing one of the key limitations of PV: intermittent energy output (Behar et al., 2021). Solar power towers (SPT) are the widely used CSP technology for providing large amounts of energy for multi-generation purposes (Roux et al., 2024). However, an SPT system has low efficiency due to the large amount of irreversibilities associated with the SPT system. Therefore, a highly efficient energy generation system that could increase the thermal performance of the overall solar plant is required (Nasouri and Delgarm, 2023).

Various researchers have developed different power generation systems to use the solar energy from the SPT system, such as the combined HBC-ORC-vapor absorption cycle (Zhou et al., 2023), the combined cascaded supercritical $CO_2$ ($sCO_2$) Brayton cycle-ORC (Khan and Mishra, 2023a), the recompression of $sCO_2$ with compressor intercooling (Ma et al., 2019), the partial cooling $sCO_2$ cycle-ORC (Khan et al., 2024a), and the co-generation combine cycle (Adnan et al., 2022). Furthermore, the gas cycle, which uses $sCO_2$ as a working fluid, can utilize heat from different sources, such as coal, natural gas, geothermal, and solar thermal energy (Ahn et al., 2015). In this regard, several researchers, including Khan and Mishra (2021), examined the pre-compression configuration of the $sCO_2$ cycle in conjunction with ORC for utilizing the heat from SPT. They found that energy efficiency and power increased by 4.51% and 4.52%, respectively, using ORC. Qin et al. (2023) examined a combined system using recompression Brayton cycle and transcritical $CO_2$ ($tCO_2$) refrigeration for producing power and cooling utilizing the marine engine heat. They found that the waste heat recovery efficiency was 65.1%, and the coefficient of performance was 3.059. Huang et al. (2022) created a novel hybrid system using ejector cooling and the sCO2 Brayton cycle for combined cooling and power production. With R32 as the ideal fluid, the effective thermal of the suggested system was found to be 42%. Recently, Zendehnam and Pourfayaz (2024) analyzed a partial heating configuration of the $CO_2$ cycle for waste heat recovery. They conducted an advanced exergy and advanced exergoeconomic analysis of that proposed system. They concluded that the system obtained maximum exergy efficiency of 58.8% and 926.9 kW of total exergy destruction. Pan et al. (2022) examined the different configurations of the $sCO_2$ cycle for solar energy utilization. To recover waste energy, they combined this cycle with ORC. The suggested system's exergy, energy efficiency, and ecological efficiency increased to 66.91%, 41.22%, and 84.54%, respectively. To use waste heat, Zhu et al. (2022) recently developed two configurations of the $sCO_2$ Brayton cycle and Kalina cycle and another of the $sCO_2$ Brayton cycle and ORC. According to comparison data, the combined $sCO_2$ cycle and ORC thermally performed more effectively when R32 and ammonia were used. Therefore, it was seen that $CO_2$ was widely used in the gas cycle to utilize solar heat.

ORC can recover waste heat at medium and low temperatures. ORC is currently being employed as a bottoming cycle. This assertion is supported by several studies. For example, Nondy and Gogoi (2021) looked at several ORC configurations to recover waste heat, including recuperated ORC, regenerative ORC (RORC), regenerative-recuperative ORC (RRORC), and basic ORC. They discovered that the RORC outperformed the other three designs thermodynamically. The power output and energy efficiency of this arrangement are 15.33% and 16.19% higher than those of the basic ORC, respectively. Solid oxide fuel cells and gas turbine-based ORCs were investigated by Wang et al. (2022) for low-temperature heat recovery. They examined the suggested system through energy, economic, and energy-related analyses. They noticed that the system's overall energy efficiency was 92.95%. Waste heat recovery was discovered to benefit from the ORC. Mahmoud et al. (2023) looked at two ORC configurations: a regenerative ORC that uses waste heat from a diesel engine and a standard ORC. Following a thorough thermodynamic analysis, they found that, in comparison to a standalone diesel engine, thermal performance was enhanced by the regenerative ORC by 15.31% and the basic ORC by 7.98%.

In some studies, flash separators are used in ORCs instead of the different modified ORCs. That ORC is called an organic Rankine flash cycle (ORFC). Various studies have been performed using the ORFC to enhance the performance of their power generation cycle. Wu and Wang (2018) carried out a novel combined recompression supercritical $CO_2$ cycle (RSBC) and ORFC for nuclear application. They compared the performance with RSBC and ORC on the basis of thermodynamic and exergoeconomic analysis. The findings indicate that the RSBC/ORFC has up to 6.57% higher second-law efficiency and up to 3.75% lower total product unit cost than the RSBC. The RSBC-ORFC can achieve comparable or slightly lower total product unit cost and somewhat higher second-law efficiency than the RSBC-ORC. The ORFC, ORFC two-phase expander, and ORC were compared in terms of performance by Lee and Sang (2016). They found that, of the two cycles under consideration, ORFC can recover low-grade energy sources efficiently and that the cycle type or working fluid that performs at its best relies on the source temperature. Tang et al. (2023) used three configurations of the ORFCs to recover waste heat from the RSBC system, namely the basic ORFC, the regenerative, and the organic ORFC. According to the data, the RSBC-OFRC has the highest energy efficiency, which is up to 1.95% greater than the total energy efficiency of the other RSBC/ORFC combinations.

The HBC is a key component of concentrated solar power systems (SPTs) because it generates power efficiently at high temperatures. Utilizing the HBC and $tCO_2$ cycles as the bottoming cycle, Khan et al. (2023) recently suggested a unique thermodynamic combined cycle for the SPT plant's high-temperature solar energy utilization. They used an exergoeconomic and thermodynamic point of view to analyze the performance. The plant's thermal and energy efficiency were determined to be 32.39% and 34.68%, respectively, while its electricity cost was found to be 1.613 US cents per kWh. Additionally, Zhou et al. (2023) suggested a combined cycle power generation facility that would use an ORC for additional power generation and a vapor absorption system for the HBC's input cooling. The suggested combined cycle was examined from both an economic and thermodynamic perspective. To preserve food at low temperatures, Khan and Mishra (2023b) developed a unique SPT-driven trigeneration system combining an HBC for power generation with a cascaded cooling system for cooling and heating purposes. They found that the energy, exergy efficiency, and power production of the proposed plant were 28.82%, 39.53%, and 14,865 kW, respectively. Recently, Khan et al. (2024b) proposed a

novel combined HBC-ORC system to generate power from an SPT system. They analyzed that system on the basis of thermodynamic analysis along with detailed working fluid selection. The proposed system obtained the energy, exergy, and power output as 37.11%, 39.74%, and 19,135 kW using R1233zd (E) as the working fluid in the ORC.

From the literature survey, it was concluded that the Brayton cycle with helium working fluid was more efficient than the Brayton cycle with air or $sCO_2$ as working fluids in high-temperature applications such as in SPT technology. Apart from this, ORFC is much more beneficial than ORC for recovering waste heat at low temperatures. It was also concluded that the SPT-HBC system performance can be further improved by using a specific low-temperature cycle. Until now, no study has been performed using HBC and ORFC for SPT applications to enhance the overall SPT system performance. Therefore, a novel combined cycle using the HBC and ORFC to utilize the heat of the SPT system is proposed in this study. The performance of the proposed system was evaluated on the basis of thermodynamic and economic aspects using computational techniques through engineering equation software (EES). The objectives of the present work are:

- To improve the performance of the SPT-based plant by implementing the ORFC in the basic HBC for the SPT application.
- To assess the developed unique power production system's performance from economic and thermodynamic perspectives.
- To assess how well the newly constructed power generation plant performs compared to earlier research of a similar nature and the conventional SPT-HBC system.
- To do a parametric analysis on the suggested plant to investigate how various variables affect outcomes.

## 2 System description

This proposed SPT plant has three subsystems (SPT, HBC, and ORFC), as shown in Figure 1. The corresponding temperature-entropy (T-s) diagram is given in Figure 2. In the SPT system, air serves as the heat transfer fluid (HTF). Because the blower had a negligible effect on the thermodynamic characteristics, the thermodynamic properties in states 2 and 3 are essentially the same. HBCs are more efficient than $CO_2$ Brayton cycles because helium performs better than $CO_2$ in solar power plants with central receivers (at high temperatures) (Dunham and Iverson, 2014). Its low specific gravity and chemical inertness are two noteworthy characteristics. Furthermore, helium has a thermal conductivity that is six to nine times higher than that of $CO_2$ and air, respectively (Dunham and Iverson, 2014).

After taking the heat through the intermediate exchanger (IHE) ($T_4$ = 850°C), the helium stream passes through the Turbine-1 (T1), where it gives the work (process 7–8). From state 8, the helium stream passes through the recuperator (process 8–9), where it transfers the heat to the low-temperature helium stream. At point 9, the temperature is 204.1°C, which indicates that heat is still present. The organic Rankine flash cycle (ORFC) is utilized to improve system performance and consume much heat. The heat recovery vapor generator (HRVG) in the ORFC absorbs the residual heat (process 9–10). The temperature of the helium stream drops to approximately 31.16°C ($T_9$) after the HRVG. This stream passes through the precooler (states 10 to 4) and is compressed in the compressor (states 4–5). This compressed stream passes through the recuperator to take some heat, and then it passes through the IHE (states 5–6). The ORFC takes heat through the HRVG and passes through Expansion Valve-1 (EV1) at a temperature of 181.1°C ($T_{13}$). After this, the wet stream of organic fluid goes to the flash separator (FS), where liquid and vapor are separated. The vapor stream goes to Turbine-2 and is expanded (process 15–16). However, from the FS, the liquid passes through Expansion Valve-2 (EV2) and mixes with liquid that comes from the T2 in the mixer. After the mixer, the saturated whole saturated liquid at state 19 passes through the condenser (COND) (process 19–11). After COND, the liquid passes through the pump (process 11–12) and goes to the HRVG to take heat. In this way, the cycle repeats. Because R290 (propane) has zero ODP, a low global warming potential (GWP), and favorable thermodynamic features that make it a more ecologically friendly alternative, it has been employed as the working fluid in the ORFC and is being increasingly recognized as a future-proof working fluid (Khan and Singh, 2024).

## 3 Mathematical modeling

The following presumptions were made when the system under consideration was mathematically modeled (Equations 1–25): (1) the assumption was that every component operated in a thermodynamic steady state. (2) Table 1 lists the pressure loss in the HBC system that has been taken into account. (3) The ORFC system's pressure loss was disregarded. (4) The accompanying kinetic and potential energy have been disregarded. (5) The state of the refrigerant at the inlet of the pump and Turbine-2 is considered saturated liquid and saturated vapor, respectively.

### 3.1 Exergy and energy evaluation

Equations for the energy and exergy balance considering the component as the control volume and working on a steady-state process are presented as (Zhou et al., 2023):

$$\dot{Q}_{CV} - \dot{W}_{CV} + \sum(\dot{m}_i h_i) - \sum(\dot{m}_e h_e) = 0, \quad (1)$$

$$\dot{E}d = \dot{E}x_{in} - \dot{E}x_{out}, \quad (2)$$

where $\dot{E}x_{in}$ and $\dot{E}x_{out}$ denote, respectively, energy at the thermodynamic system's entrance and exit, as well as the component's rate of energy disintegration, which is represented by $\dot{E}d$. $\dot{Q}_{CV}$ stands for heat interactions from the control volume, and $\dot{W}_{CV}$ is work interactions. Chemical exergy has been disregarded because the current approach ignores changes in chemical concentration. The assumptions also overlook exergy resulting from height and velocity. As a result, total exergy solely includes physical exergy and is defined as (Zhou et al., 2023; Khan and Singh, 2024):

$$\dot{E}x_j = \dot{m}\cdot\left[\left(h_j - h_0\right) - T_0\left(s_j - s_0\right)\right]. \quad (3)$$

The governing equations of the thermodynamic modeling of the SPT-HBC-ORFC are given in Table 2.

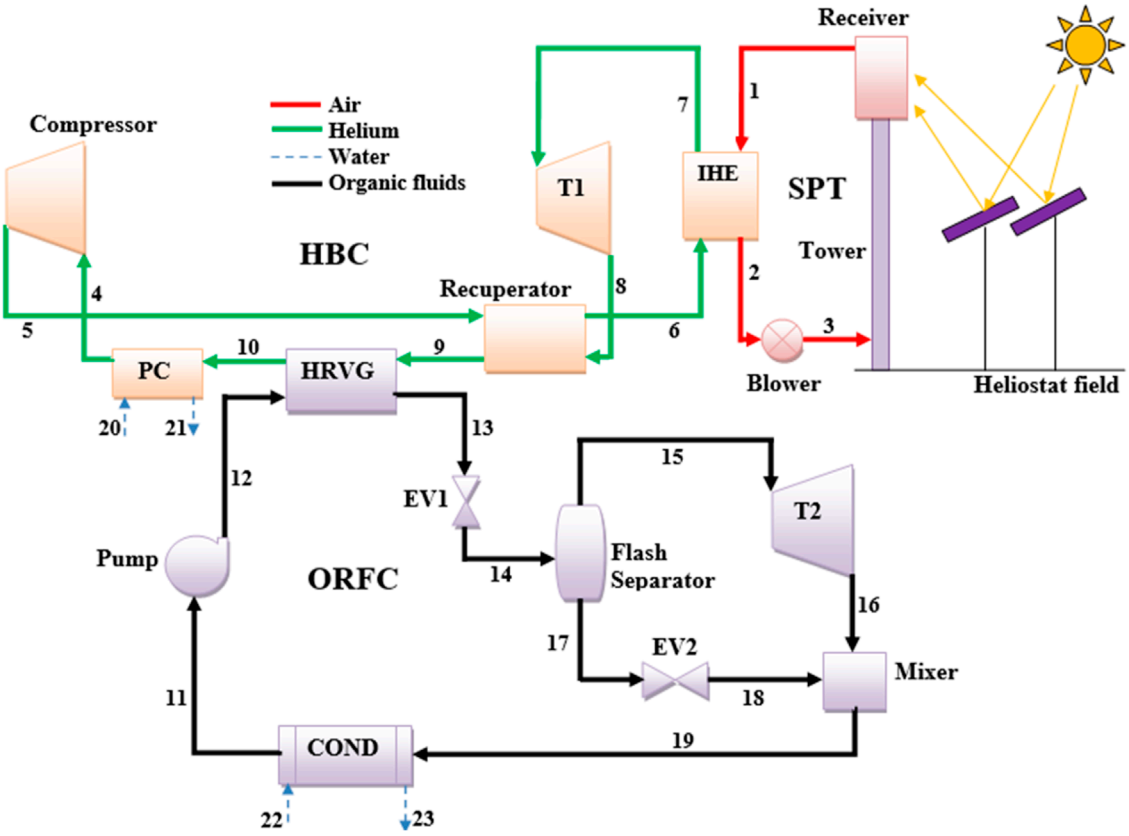


FIGURE 1
Schematic diagram of the SPT-HBC-ORFC power generation plant.

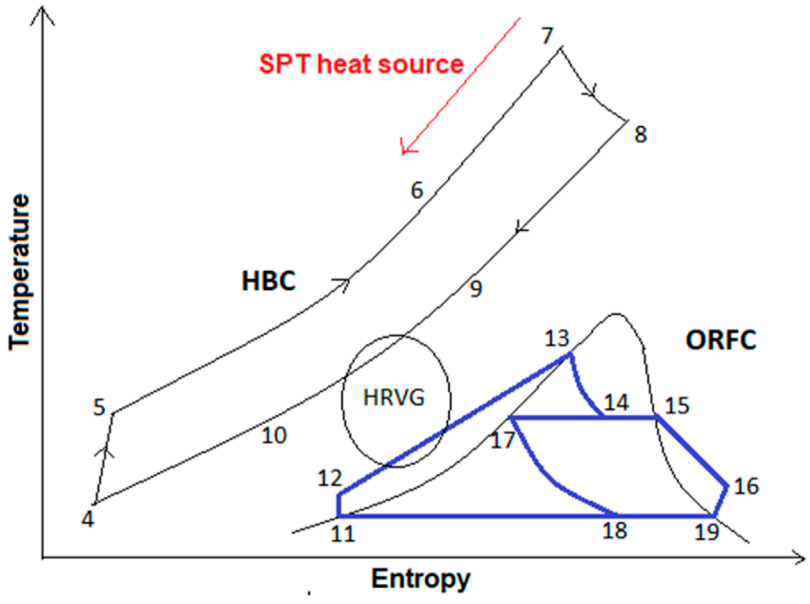


FIGURE 2
Corresponding T-s diagram of the proposed power generation plant.

TABLE 1 Design parameters and data for simulation.

| Parameter | Value |
|---|---|
| **SPT** | |
| Number of heliostats ( $N_{hel}$) | 500 [6] |
| Sun apparent temperature ( $T_{Sun}$) | 4500 K [6] |
| Area of heliostat ( $A_{hel}$) | 9.45 × 12.84 $m^2$ [6] |
| DNI | 850 $W/m^2$ [6,9] |
| Aperture area of receiver ( $A_r$) | 68.1 $m^2$ [6] |
| Heliostat field efficiency ( $\eta_{hel}$) | 0.75 [6] |
| Receiver efficiency ($\eta_r$) | 0.9 [6] |
| Maximum temperature obtained from SPT ($T_1$) | 1,125 °C [9] |
| **HBC** | |
| Inlet pressure of the compressor ($P_4$) | 2,500 kPa [6,9] |
| Maximum temperature of HBC ($T_7$) | 850 °C [6,9] |
| Isentropic efficiency of the compressor ( $\eta_{comp}$) | 0.88 [6,9] |
| Turbine-1 efficiency ( $\eta_{T1}$) | 0.9 [6,9] |
| Compressor pressure ratio (PR) | 2.237 |
| Heat exchangers effectiveness ($\varepsilon$) | 0.9 [6,9] |
| Pressure loss in IHE | 2% [9] |
| **ORFC** | |
| Isentropic efficiency of Turbine-2 ( $\eta_{T2}$) | 0.85 [18, 23] |
| Isentropic efficiency of both pumps ( $\eta_{pump}$) | 0.85 [18,23] |
| Working fluid | R290 |
| HRVG pinch point | 15°C |
| Condenser temperature | 30°C [18] |
| Condenser pinch point | 10°C [18] |
| Atmospheric temperature ( $T_0$) | 25°C |
| Atmospheric pressure ( $P_0$) | 101.3 kPa |

### 3.1.1 Solar subsection modeling

The solar subsystem consists only of heliostats and receivers as the main components. Hundreds of heliostats get energy from the sun through solar radiation or incident direct normal irradiance (DNI). The heliostat area, number, and DNI (which varies depending on the earth's location and time) determine the total amount of solar radiation that the heliostats receive. As a result, the solar heat received by the heliostats can be written as (Zhou et al., 2023):

$$\dot{Q}_{Sun} = DNI \cdot A_{hel} \cdot N_{hel}, \tag{4}$$

where and $N_{hel}$ and $A_{hel}$ represent the number of heliostats and the aperture area of each heliostat, respectively.

The actual amount of solar heat from the heliostats reached the receiver depends on the efficiency of the heliostat field. Some amount of the solar heat is lost to the environment. Therefore, the actual amount of solar heat that reaches the receiver from the heliostat field is expressed as (Zhou et al., 2023):

$$\dot{Q}_{rec,in} = \eta_{hel} \cdot \dot{Q}_{Sun}, \tag{5}$$

where $\eta_{hel}$ represents heliostat efficiency, which depends on the different optical parameters given by Khan et al. (2023). It is important to emphasize that we do not attempt to compute this value in the current research. However, the value has been taken from an already-running SPT plant. The receiver loses some amount of heat due to the different heat transfer losses. Therefore, the net amount of the solar heat absorbed by the receiver through HTF is expressed as (Zhou et al., 2023):

$$\dot{Q}_{rec,net} = \dot{Q}_{rec,in} - \dot{Q}_{rec,loss}, \tag{6}$$

$$\dot{Q}_{rec,net} = \dot{m}_{air} \cdot (h_1 - h_3). \tag{7}$$

Therefore, the receiver efficiency can be determined as follows (Zhou et al., 2023; Khan and Singh, 2024):

$$\eta_{rec} = \frac{\dot{Q}_{rec,net}}{\dot{Q}_{rec,in}}. \tag{8}$$

### 3.1.2 Efficiency assessment

The energy efficiency and exergy efficiency of the studied solar power plant (SPT-HBC-ORFC) have been represented as follows (Zhou et al., 2023):

$$\eta_{en,Plant} = \frac{\dot{W}_{net,comb}}{\dot{Q}_{Sun}}, \tag{9}$$

$$\eta_{ex,Plant} = \frac{\dot{W}_{net,comb}}{\dot{Q}_{Sun} \cdot \left(1 - \frac{T_0}{T_{Sun}}\right)}, \tag{10}$$

where $T_{Sun}$ is the sun's apparent temperature. $\dot{W}_{net,comb}$ is the net power output obtained through the combined cycle (HBC-ORFC) and can be expressed as

$$\dot{W}_{net,comb} = \dot{W}_{T1} - \dot{W}_{comp} + \dot{W}_{net,ORFC}, \tag{11}$$

where $\dot{W}_{net,ORFC}$ is the net power output from the ORFC and can be expressed as:

$$\dot{W}_{net,ORFC} = \dot{W}_{T2} - \dot{W}_{pump}. \tag{12}$$

Moreover, the energy efficiency and exergy efficiency of the combined HBC-ORFC are calculated as (Zhou et al., 2023; Nondy and Gogoi, 2021):

$$\eta_{en,comb} = \frac{\dot{W}_{net,comb}}{\dot{Q}_{IHE}}, \tag{13}$$

$$\eta_{ex,comb} = \frac{\dot{W}_{net,comb}}{(\dot{E}x_1 - \dot{E}x_2)}, \tag{14}$$

where $(\dot{E}x_1 - \dot{E}x_1)$ refers to the exergy input through IHE in the HBC (Zhou et al., 2023; Nondy and Gogoi, 2021).

TABLE 2 Mathematical equations for modeling.

| Component | Energetic evaluation | Exergetic evaluation |
|---|---|---|
| Heliostat field | $\dot{Q}_{recin} = \eta_{field} \cdot DNI \cdot A_{hel} \cdot N_{hel}$ | $\dot{Q}_{Sun} \cdot \left(1 - \frac{T_0}{T_{Sun}}\right) = \dot{Q}_{rec,in} \cdot \left(1 - \frac{T_0}{T_{hel}}\right) + \dot{E}d_{hel}$ |
| Receiver | $\dot{Q}_{rec,in} = \dot{m}_{air} \cdot (h_1 - h_3) + \dot{Q}_{rec,loss}$ | $\dot{E}x_3 + \dot{Q}_{rec,in} \cdot \left(1 - \frac{T_0}{T_{hel}}\right) = \dot{E}x_1 + \dot{Q}_{rec,loss} \cdot \left(1 - \frac{T_0}{T_{rec}}\right) + \dot{E}d_{rec}$ |
| IHE | $\dot{Q}_{IHE} = \dot{m}_{air} \cdot (h_1 - h_2) + \dot{m}_{He} \cdot (h_7 - h_6)$ | $\dot{E}x_1 - \dot{E}x_2 = \dot{E}x_7 - \dot{E}x_6 + \dot{E}dc4_{\mathrm{IHE}}$ |
| Turbine-1 | $\dot{W}_{T1} = \dot{m}_{He} \cdot (h_7 - h_8)$<br>$\eta_{T1} = \frac{(h_7 - h_8)}{(h_7 - h_{8s})}$ | $\dot{E}x_7 = \dot{E}x_8 + \dot{W}_{T1} + \dot{E}d_{T1}$ |
| Compressor | $\dot{W}_{comp} = \dot{m}_{He} \cdot (h_4 - h_5)$<br>$\eta_{comp} = \frac{(h_{5s} - h_4)}{(h_5 - h_4)}$ | $\dot{E}x_4 = \dot{E}x_5 - \dot{W}_{comp} + \dot{E}d_{comp}$ |
| Recuperator | $(h_8 - h_9) = (h_6 - h_5)$<br>$\varepsilon_{Recuperator} = \frac{(T_3 - T_2)}{(T_5 - T_2)}$ | $\dot{E}x_5 - \dot{E}x_6 = \dot{E}x_3 - \dot{E}x_2 + \dot{E}d_{Recuperator}$ |
| Precooler | $\dot{m}_{air} \cdot (h_{10} - h_4) = \dot{m}_{water} \cdot (h_{21} - h_{20})$ | $\dot{E}x_{10} - \dot{E}x_4 = \dot{E}x_{21} - \dot{E}x_{20} + \dot{E}d_{PC}$ |
| HRVG | $\dot{m}_{He} \cdot (h_9 - h_{10}) = \dot{m}_{of} \cdot (h_{13} - h_{12})$ | $\dot{E}x_9 - \dot{E}x_{10} = \dot{E}x_{13} - \dot{E}x_{12} + \dot{E}d_{HRVG}$ |
| Turbine-2 | $\dot{W}_{T2} = \dot{m}_{of} \cdot (h_{15} - h_{16})$<br>$\eta_{T2} = \frac{(h_{15} - h_{16})}{(h_{15} - h_{16s})}$ | $\dot{E}x_{15} = \dot{E}x_{16} + \dot{W}_{T2} + \dot{E}d_{T2}$ |
| Flash separator | $\dot{m}_{of} \cdot h_{14} = \dot{m}_{15} \cdot h_{15} + \dot{m}_{17} \cdot h_{17}$<br>$\dot{m}_{of} = \dot{m}_{15} + \dot{m}_{17}$ | $\dot{E}x_{14} = \dot{E}x_{15} + \dot{E}x_{17} + \dot{E}d_{FS}$ |
| Condenser | $\dot{m}_{of} \cdot (h_{19} - h_{11}) = \dot{m}_{water} \cdot (h_{23} - h_{22})$ | $\dot{E}x_{19} - \dot{E}x_{11} = \dot{E}x_{23} - \dot{E}x_{22} + \dot{E}d_{COND}$ |
| Pump | $\dot{W}_{Pump} = \dot{m}_{of} \cdot (h_{11} - h_{11})$<br>$\eta_{Pump} = \frac{(h_{12s} - h_{11})}{(h_{12} - h_{11})}$ | $\dot{E}x_{11} = \dot{E}x_{12} - \dot{W}_{Pump} + \dot{E}d_{Pump}$ |
| Expansion valve-1 | $h_{13} = h_{14}$ | $\dot{E}x_{13} = \dot{E}x_{14} + \dot{E}d_{EV1}$ |
| Expansion valve-1 | $h_{17} = h_{18}$ | $\dot{E}x_{17} = \dot{E}x_{18} + \dot{E}d_{EV2}$ |
| Mixer | $\dot{m}_{of} \cdot h_{19} = \dot{m}_{16} \cdot h_{16} + \dot{m}_{18} \cdot h_{18}$<br>$\dot{m}_{of} = \dot{m}_{16} + \dot{m}_{18}$ | $\dot{E}x_{19} = \dot{E}x_{18} + \dot{E}x_{16} - \dot{E}d_{Mixer}$ |

Similarly, the standalone HBC efficiencies can be expressed as (Zhou et al., 2023; Nondy and Gogoi, 2021):

$$\eta_{\mathrm{en,HBC}} = \frac{\dot{W}_{\mathrm{HBC}}}{\dot{Q}_{\mathrm{IHE}}}, \tag{15}$$

$$\eta_{\mathrm{ex,HBC}} = \frac{\dot{W}_{\mathrm{HBC}}}{(\dot{E}x_1 - \dot{E}x_2)}, \tag{16}$$

where $\dot{W}_{\mathrm{HBC}}$ is net power output by the only HBC system and is expressed as:

$$\dot{W}_{\mathrm{net,HBC}} = \dot{W}_{\mathrm{T1}} - \dot{W}_{\mathrm{comp}}. \tag{17}$$

The energy efficiency and exergy efficiency of the bottoming ORFC can be defined as:

$$\eta_{\mathrm{en,ORFC}} = \frac{\dot{W}_{\mathrm{net,ORFC}}}{\dot{Q}_{\mathrm{HRVG}}}, \tag{18}$$

$$\eta_{\mathrm{ex,ORFC}} = \frac{\dot{W}_{\mathrm{net,ORFC}}}{(\dot{E}x_{13} - \dot{E}x_{12})}. \tag{19}$$

The efficiencies of the conventional (SPT-HBC) plant need to be expressed for comparison with the proposed plant (SPT-HBC-ORFC). These efficiencies can be expressed as:

$$\eta_{\mathrm{en,SPT-HBC}} = \frac{\dot{W}_{\mathrm{net,HBC}}}{\dot{Q}_{\mathrm{Sun}}}, \tag{20}$$

$$\eta_{\mathrm{ex,SPT-HBC}} = \frac{\dot{W}_{\mathrm{net,comb}}}{\dot{Q}_{\mathrm{Sun}} \cdot \left(1 - \frac{T_0}{T_{\mathrm{Sun}}}\right)}. \tag{21}$$

## 3.2 Economic evaluation

The thermodynamic analysis of any system solely considers the energy conversion, as stated by the first law, and the available exergy, as determined by the second law. Any system that is designed with economics in mind is less complicated, more efficient, and more affordable.

TABLE 3 Capital cost function of each component of the proposed plant.

| Components | Capital cost function |
|---|---|
| Heliostat | $Z_{hel} = 126 \cdot A_{hel} \cdot N_{hel}$ Zhou et al. (2023) |
| Receiver | $Z_r = A_r \cdot (79 \cdot T_{21} - 42000)$ Zhou et al. (2023) |
| IHE | $Z_{IHE} = 12000 \cdot \left(\frac{A_{IHE}}{100}\right)^{0.6}$ Bejan et al. (1996) |
| Turbine-1 | $Z_{T1} = \frac{479.3 \cdot \dot{m}_{He}}{0.93 - \eta_{T1}} \cdot \ln\left(\frac{P_4}{P_5}\right) \cdot (1 + \exp(0.036 \cdot T_4 - 54.4))$ Zhou et al. (2023) |
| Recuperator | $Z_{Recuperator} = 2681 \cdot \left(A_{Recuperator}\right)^{0.59}$ Bejan et al. (1996) |
| Precooler | $Z_{PC} = 2143 \cdot (A_{PC})^{0.514}$ Zhou et al. (2023) |
| Compressor | $Z_{comp} = \frac{71.1 \cdot \dot{m}_{He}}{0.91 - \eta_{comp}} \cdot \left(\frac{P_2}{P_1}\right) \cdot \ln\left(\frac{P_2}{P_1}\right)$ Zhou et al. (2023) |
| HRVG | $Z_{HRVG} = 309.143 \cdot (A_{HRVG})^{0.59} + 231.195$ Nondy and Gogoi (2021) |
| Turbine-2 | $Z_{T2} = 6000 \cdot (\dot{W}_{T2})^{0.7}$ Nondy and Gogoi (2021); Tang et al. (2023) |
| Flash separator | $Z_{COND} = 140 \cdot \dot{m}_{14}$ Tang et al. (2023) |
| Condenser | $Z_{COND} = 130 \cdot (A_{COND}/0.093)^{0.78}$ Nondy and Gogoi (2021); Tang et al. (2023) |
| Pump-1 | $Z_{Pump1} = 1120 \cdot \left(\dot{W}_{pump1}\right)^{0.8}$ Nondy and Gogoi (2021); Tang et al. (2023) |
| Expansion valve-1 | $Z_{EV1} = 114.5 \cdot \dot{m}_{13}$ Tang et al. (2023) |
| Expansion valve-2 | $Z_{EV2} = 114.5 \cdot \dot{m}_{17}$ Tang et al. (2023) |

The cost rate per unit hours associated with each component is expressed as (Nondy and Gogoi, 2021; Bejan et al., 1996);

$$\dot{Z}_j = \frac{Z_j \cdot CRF \cdot \varphi}{3600 \cdot N}, \tag{22}$$

where $Z_j$, "N," and $\varphi$ are capital costs of the component, annual operating hours [taken as 7,446 h (Mehrpooya et al., 2017)], and maintenance factor [taken as 1.06 (Mehrpooya et al., 2017)], respectively. The capital recovery factor (CRF) can be calculated as (Zhou et al., 2023; Nondy and Gogoi, 2021; Bejan et al., 1996):

$$CRF = \frac{i \cdot (1+i)^n}{(1+i)^n - 1}, \tag{23}$$

where "n" represents the system's life, taken as 20 years, and "i" is the rate of interest, which is 12% (Zhou et al., 2023). The capital cost of each component is also shown in Table 3.

The economic feasibility of the power generation plant is calculated by evaluating the total cost rate of the plant. The cost rates for the conventional SPT-HBC system ($\dot{C}_{SPT-HBC}$) and the proposed plant ($\dot{C}_{Plant}$) were evaluated by the following formula (Bejan et al., 1996):

$$\dot{C}_{SPT-HBC} = \dot{Z}_{SPT-HBC} + \dot{C}_{fuel}, \tag{24}$$

$$\dot{C}_{Plant} = \dot{Z}_{Plant} + \dot{C}_{fuel}, \tag{25}$$

where $\dot{Z}_{Plant}$ and $\dot{Z}_{SPT-HBC}$ are some of the cost rates of each component of the overall plant (SPT-HBC-ORFC) and conventional SPT-HBC, respectively. However, $\dot{C}_{fuel}$ is the cost of fuel. It refers to the cost of the sun, which is assumed to be zero.

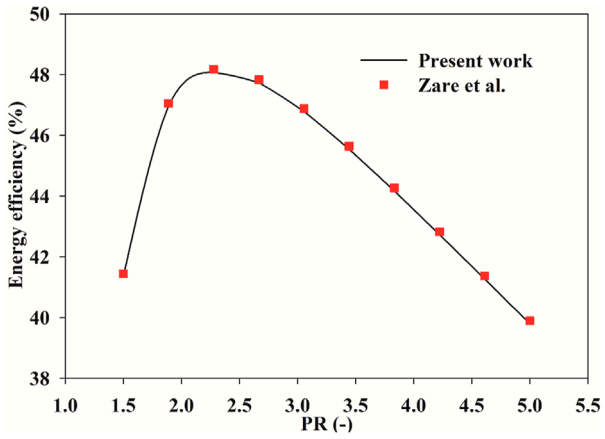


FIGURE 3
Validation of the HBC system.

# 4 Results and discussions

## 4.1 System validation

The outcomes of the two systems (HBC and ORFC) are compared and verified with data from the literature to verify the modeling technique. In Figure 3, the energy efficiency for the single HBC acquired in the present study is compared with that published by Zare et al. (2015). The ORFC parameters are validated with the

TABLE 4 Validation results of the ORFC[a].

| Parameter | Wu and Wang (2018) | Present work | Deviation (%) |
|---|---|---|---|
| Net work output (kW) | 22.79 | 22.81 | +0.08 |
| Exergy destruction (kW) | 63.67 | 63.68 | +0.01 |
| Energy efficiency (%) | 5.33 | 5.35 | +0.37 |
| Exergy efficiency (%) | 26.36 | 26.31 | −0.18 |

[a] $T_{13}$ = 135°C, $T_{11}$ = 40°C, $\eta_{T2}$ = 0.80, $\eta_{pump}$ = 0.80, $T_{14}$ = 80°C, R245fa.

study published by Wu and Wang (2018), as shown in Table 4, at the same baseline conditions. The results obtained from the present work are very close to the published data.

## 4.2 Results at base conditions

In the present study, an exergy-energy and economic analysis of the SPT-based plant were carried out using computational techniques in EES software. The EES is a modeling and simulation software developed by Klein (2018). Table 5 lists the state-point thermodynamic properties, which were determined using the EES's built-in property function. Table 6 lists the useful outcomes of the present power generation systems. A conventional SPT-HBC system has energy and exergy efficiencies of 28.23% and 30.23%, respectively. The proposed plant (SPT-HBC-ORFC) had energy and exergy efficiencies of 37.74% and 40.42%, respectively. Therefore, the energy and exergy efficiency of the proposed plant are higher than those of the conventional system. This is due to the effective utilization of the waste heat recovery coming from the SPT-HBC conventional system by extra power production through ORFC. The extra net power produced by ORFC is 4,906 kW. Therefore, by implementing the ORFC in the conventional SPT-HBC system, the energy and exergy efficiency of the proposed plant were enhanced by 33.68% and 33.70%, respectively. Furthermore, power output was obtained by the conventional system and proposed system of 14,558 kW and 19,464 kW, respectively. It means that by implementing the ORFC, the power output will be enhanced by 33.69% through the proposed plant. The energy and exergy efficiencies of the standalone HBC system are found to be 41.82% and 57.01%, respectively. However, overall plant efficiencies were reduced. This is due to the performance of the SPT system being considered. Many irreversibilities were associated with the SPT components only (i.e., heliostats and receivers).

Exergy destruction for each component has also been calculated to investigate the weakest component from an exergetic point of view. Heliostats were found to be the most exergy-destructive component, followed by the receiver, as shown in Figure 4. Because the heliostats receive heat at high temperatures from the sun, the highest exergy destruction was found in that heliostats alone contribute 39% of the total exergy destruction (28,688 kW). However, the receiver was found to be the second-highest exergy destruction component, accounting for 34.85% of total exergy destruction, because the receiver receives the heat from the heliostats at a very high temperature, which leads to high exergy destruction. The total cost rates of the conventional (SOFC-GT) plant and the proposed plant were 252.10 $/h and 291.10 $/h, respectively. Therefore, the enhancement in the cost of the proposed plant was 15.47%. This increase in the cost is due to the extra components of the ORFC. However, thermal performance is far better than that of the conventional system. Therefore, this cost increase can be justified.

## 4.3 Parametric analysis

In this section, a parametric analysis of the proposed system has been performed to investigate the impact of the different variables on performance. It is assumed that while investigating the effect of any one variable, other variables were kept constant.

### 4.3.1 Effect of compressor pressure ratio

The compressor pressure ratio (PR) is the prime factor that affects system performance. The energy and exergy efficiency of the plant first increased and reached the optimum point, then decreased. These efficiencies first increase to the compressor pressure ratio of 2.238, then decrease. The explanation is that at a PR of less than 2.237, the turbine work is dominant over the compressor work; therefore, network output increases continuously. Apart from this, after the optimum value of the compressor pressure ratio, the compressor work increases faster than the turbine work; therefore, power output decreases with the PR. The maximum energy efficiency, exergy efficiency, and power output of the proposed plant were obtained as 37.74%, 40.42%, and 19,464 kW, respectively, at a PR of 2.237. However, maximum energy efficiency, exergy efficiency, and power output of the conventional SPT-HBC plant were obtained as 28.23%, 30.23%, and 14,558 kW, respectively, at a PR of 2.237, as shown in Figure 5A. Apart from this, the total cost rate of both systems is shown in Figure 5B. The total cost rate of the conventional SPT-HBC system increases with the PR. Because the PR increases the temperature at the outlet of the compressor, high-strength and quality material is required for compressor design. The capital cost function for the compressor depicts the same thing. The total cost of the conventional SPT-HBC system increases from 248.2 $/h to 260.9 $/h as PR increases from 1.5 to 5. However, the cost rate of the proposed plant follows the reverse trend of work output and efficiencies. The total cost rate of the proposed plant first decreased

TABLE 5 Thermodynamic properties at each state.

| State | Working fluid | Temperature (°C) | Pressure (kPa) | Mass flow rate (kg/s) | Total exergy (kW) |
|---|---|---|---|---|---|
| 1 | Air | 1,125 | 101.30 | 57.09 | 41,036 |
| 2 | Air | 600.40 | 101.30 | 57.09 | 15,499 |
| 3 | Air | 600.40 | 101.30 | 57.09 | 15,499 |
| 4 | Helium | 30 | 2,500 | 22.39 | 44,618 |
| 5 | Helium | 160.90 | 5,593 | 22.39 | 58,762 |
| 6 | Helium | 550.40 | 5,513 | 22.39 | 81,631 |
| 7 | Helium | 850 | 5,473 | 22.39 | 105,591 |
| 8 | Helium | 593.50 | 2,630 | 22.39 | 74,427 |
| 9 | Helium | 204.10 | 2,580 | 22.39 | 49,572 |
| 10 | Helium | 31.16 | 2,540 | 22.39 | 45,542 |
| 11 | R290 | 35 | 101.30 | 32.56 | 4,468 |
| 12 | R290 | 41.16 | 2026 | 32.56 | 4,571 |
| 13 | R290 | 189.10 | 2026 | 32.56 | 7,420 |
| 14 | R290 | 183 | 810.40 | 32.56 | 5,831 |
| 15 | R290 | 183 | 810.40 | 65.47 | 7,220 |
| 16 | R290 | 42.10 | 101.30 | 65.47 | 1,041 |
| 17 | R290 | 183 | 810.40 | 32.90 | 387 |
| 18 | R290 | 42.10 | 101.30 | 32.90 | 309 |
| 19 | R290 | 109.70 | 101.30 | 32.56 | 640.50 |
| 20 | Water | 25 | 101.30 | 170.10 | 0 |
| 21 | Water | 35 | 101.30 | 170.10 | 116.40 |
| 22 | Water | 25 | 101.30 | 537.20 | 0 |
| 23 | Water | 35 | 101.30 | 537.20 | 368.30 |

to a PR of 2.237, then increased continuously. Its lowest value was observed as 291.1$/h at a PR of 2.237.

### 4.3.2 Effect of the compressor inlet temperature

As seen in this study, the compressor inlet temperature is controlled through the precooler. Therefore, it is necessary to examine the effect of the compressor inlet temperature on performance to know whether inlet cooling is required. Figures 6A, B illustrate the relationship between the compressor inlet temperature and thermal performance. As the compressor temperature rises, the combined cycle's power production falls. The compressor's enthalpy difference rises, which causes the compressor's work to rise as well and reduces the combined cycle's power production. This indicates that as the compressor inlet temperature rises, the power plant's energy and exergy efficiency likewise somewhat decline. Alternatively, as the compressor inlet temperature increases, it reduces the density of the helium fluid, which leads to occupying more space; consequently, the compression work is increased. The result is a reduction in the net power output from the cycle. As the compressor temperature rose from 30°C to 40°C, the energy and exergy efficiency and power output of the proposed plant fell from 37.74% to 37.56%, from 40.42% to 40.23%, and from 19,464 kW to 19,370 kW, respectively. However, as the compressor temperature rose from 30°C to 40°C, the energy and exergy efficiency and power output of the conventional SPT-HBC system fell from 28.23% to 27.39%, from 30.23% to 29.33%, and from 14,558 kW to 14,124 kW, respectively. Apart from thermodynamic performances, the system's total cost rate

TABLE 6 Calculated outcomes from the hybrid plant at base conditions.

| Parameter | Conventional plant (SPT-HBC) | Proposed plant (SPT-HBC-ORFC) |
|---|---|---|
| $\dot{W}_{net,HBC}$ (kW) | 14,558 | 14,558 |
| $\eta_{en,HBC}$ (%) | 41.82 | 41.82 |
| $\eta_{ex,HBC}$ (%) | 57.01 | 57.01 |
| $\dot{W}_{net,ORFC}$ (kW) | — | 4,906 |
| $\eta_{en,ORFC}$ (%) | — | 17.93 |
| $\dot{W}_{net,overall}$ (kW) | 14,558 | 19,464 |
| $\eta_{en,overall}$ (%) | 28.23 | 37.74 |
| $\eta_{ex,overall}$ (%) | 30.23 | 40.42 |
| $\dot{E}d_{overall}$ (kW) | 33,595 | 28,688 |
| $\dot{C}_{Plant}$ ($/h) | 252.10 | 291.10 |

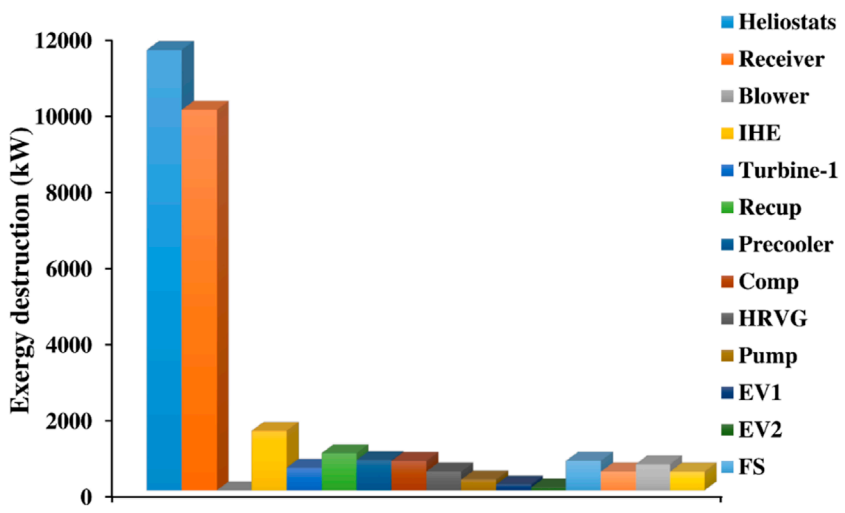


FIGURE 4
Exergy destruction for each component.

is shown in Figure 5B. It can be seen that the total rate of the conventional SPT-HBC system is not affected by the compressor inlet temperature. However, the total cost rate of the proposed plant increases slightly with compressor inlet temperature. It follows the reverse trend of the power output due to the capital cost function relationship of the different components of the ORFC system. The total cost rate of the proposed plant (SPT-HBC-ORFC) slightly increased from 291.1 $/h to 292.8 $/h as the compressor temperature rose from 30°C to 40°C.

### 4.3.3 Effect of the Turbine-1 inlet temperature

The energy efficiency, exergy efficiency, and power output of the overall solar power plant increased with the Turbine-1 inlet temperature because the increased inlet temperature increased the enthalpy difference across the turbine, which led to an increase in the net power output. Consequently, turbine work output increased. However, the compressor work is not affected. Therefore, net workout output increased. Alternatively, the turbine inlet temperature is the highest temperature of the cycle and is considered the heat source temperature. Therefore, the thermal efficiency increases with the heat source temperature at the fixed sink temperature according to the definition. The energy efficiency, exergy efficiencies, and power output of the proposed power plant increased from 30.57% to 39.25%, from 32.74% to 42.04%, and from 15,763 kW to 20,242 kW, respectively, as seen in Figures 7A, B, as the inlet temperature increased from 550°C to 950°C. However, energy efficiency, exergy efficiency, and power output of the SPT-HBC system increased from 18.42% to 30.29%, from 19.73% to

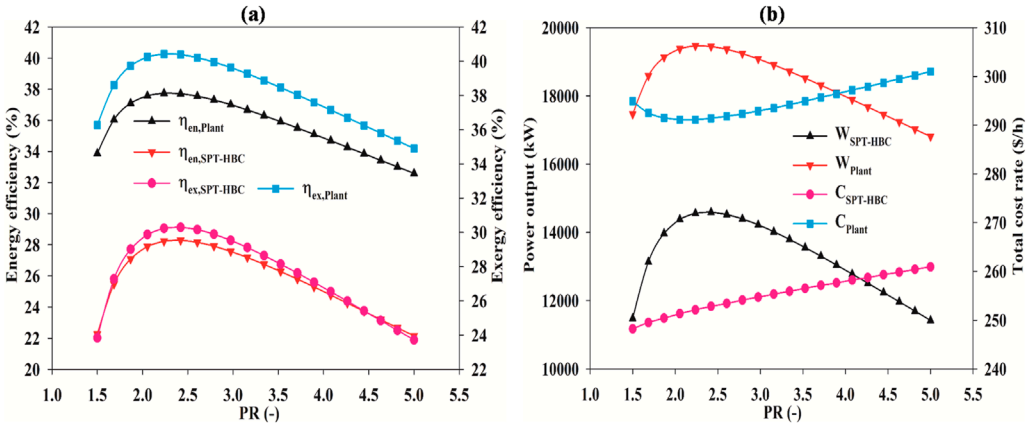


FIGURE 5
Effect of compressor pressure ratio on **(A)** efficiencies, **(B)** power output and total cost.

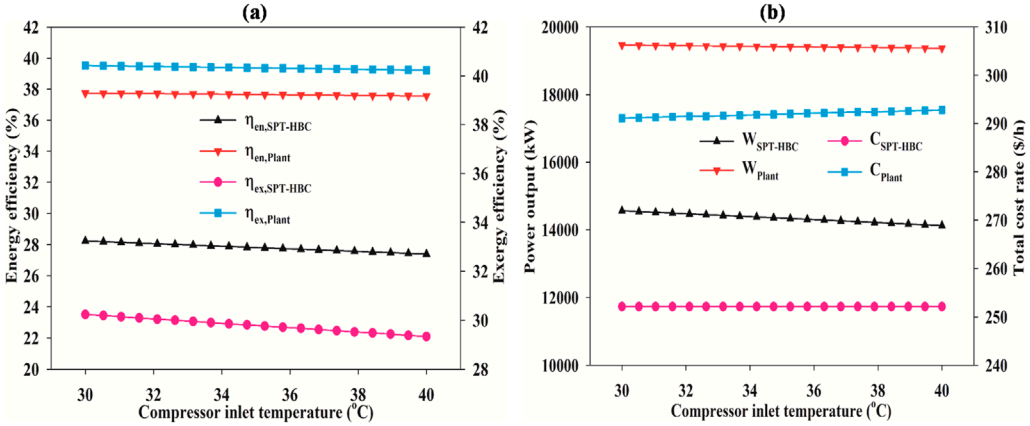


FIGURE 6
Effect of compressor inlet temperature on **(A)** efficiencies, **(B)** power output and total cost.

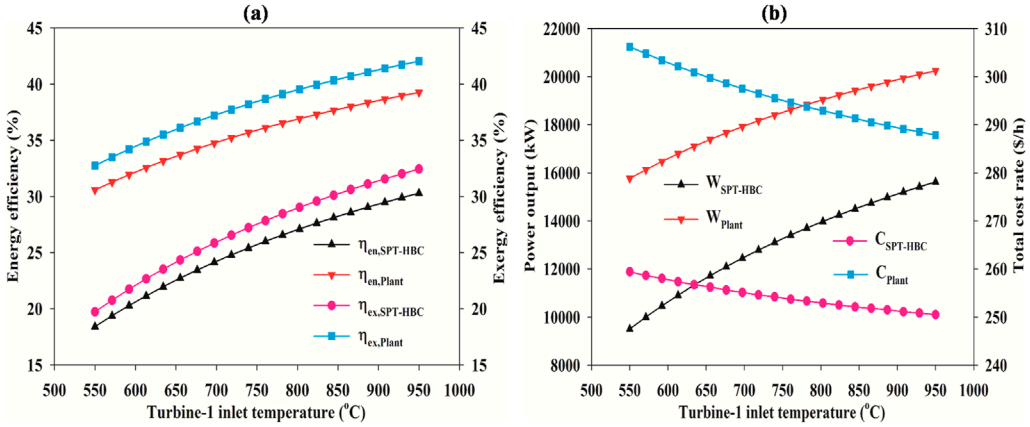


FIGURE 7
Effect of turbine-1 inlet temperature on **(A)** efficiencies, **(B)** power output and total cost.

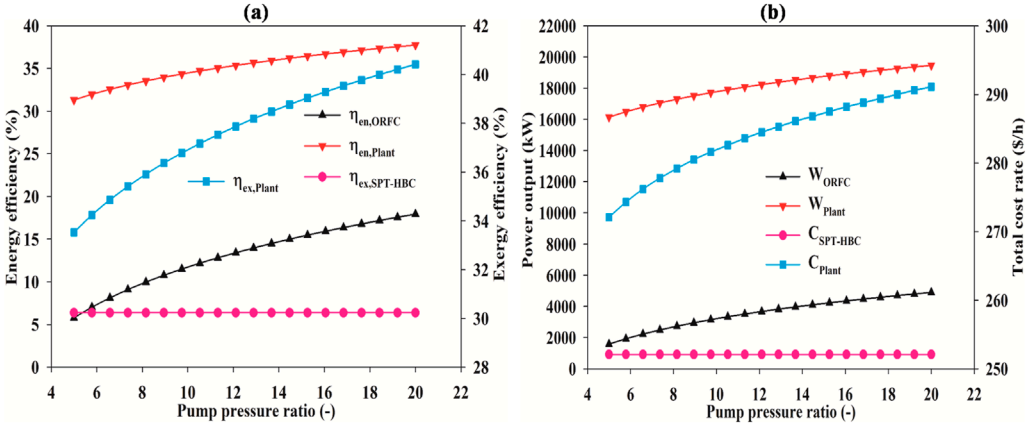


FIGURE 8
Effect of pump pressure ratio on **(A)** efficiencies, **(B)** power output and total cost.

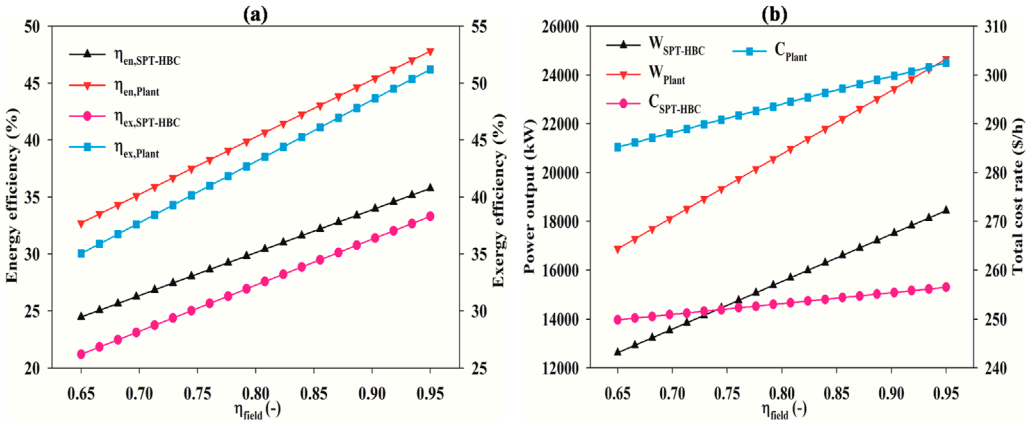


FIGURE 9
Effect of heliostat field efficiency on **(A)** efficiencies, **(B)** power output and total cost.

32.44%, and from 9,500 kW to 15,619 kW, respectively, as the inlet temperature increased from 550°C to 950°C. Figure 7B also shows that the total cost rate of both systems decreased with Turbine-1 inlet temperature. It has a reverse trend in terms of work output and energy-exergy efficiency. The capital cost of the components decreased with the Turbine-1 inlet temperature. The increase in the overall cost rate at the upper limits of Turbine-1's intake temperature can be ascribed to Turbine-1's increased investment costs as its inlet temperature rises, which are not offset by an increase in power generated. The total cost rate of the conventional SPT-HBC system and proposed plant decreased from 259.4 $/h to 250.5 $/h and from 306.2 $/h to 287.8 $/h, respectively, as the inlet temperature increased from 550°C to 950°C.

### 4.3.4 Effect of pump pressure ratio

Pump inlet pressure is influenced by ambient conditions. However, the outlet pressure needs to be set, which depends on the pump pressure ratio. The pump pressure ratio is the controllable parameter in the present study. It affects the cycle performance. In this section, the effect of the pump pressure ratio was examined. The exergy efficiency, energy efficiency, and power output of the proposed plant and the energy efficiency of the ORFC system increased with the pump pressure ratio, as shown in Figures 8A, B. An increasing pump pressure ratio increases the enthalpy difference across Turbine-2, resulting in a net enhancement in the net power output. That leads to improvements in the energy efficiency of the ORFC and the overall proposed plant. The energy efficiency and power output of the ORFC increased from 5.78% to 17.93% and from 1,586 kW to 4,906 kW, respectively, as the pump pressure ratio increased from 5 to 20. However, the energy, exergy efficiency, and power output of the proposed power plant increased from 31.31% to 37.74%, from 33.53% to 40.42%, and from 16,144 kW to 19,464 kW, respectively, within the range of the pressure ratio. Figure 8B also shows that the cost of the overall proposed plant increased with the pump pressure ratio. However, the cost of the conventional system is not affected by the pump pressure ratio. The cost rate of the proposed plant increased from 272.1 $/h to 291.1 $/h. It follows the same trend as the power output.

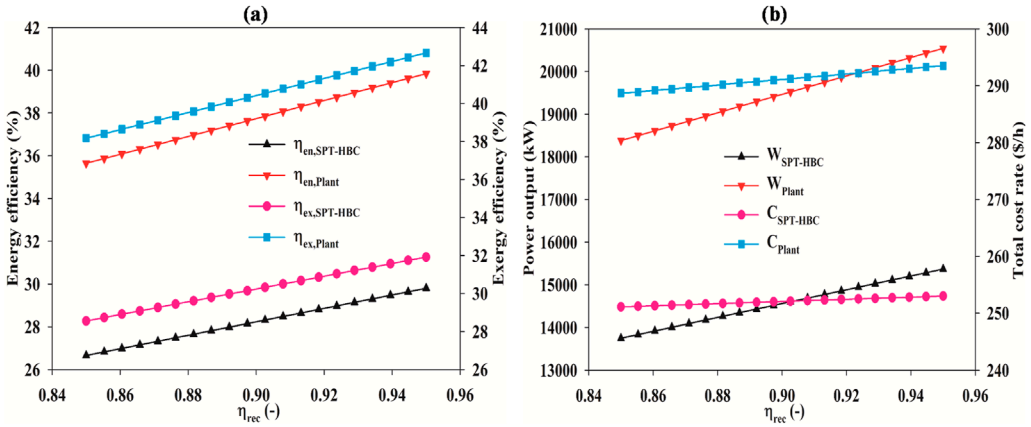


FIGURE 10
Effect of receiver efficiency on **(A)** efficiencies, **(B)** power output and total cost.

TABLE 7 Performance comparison with earlier studies.

| Systems | DNI ($W/m^2$) | $\eta_{field}$ | $\eta_{field} \times \eta_{rec}$ | $\eta_{rec}$ | $\eta_{en,comb}$ (%) | $\eta_{en,Plant}$ (%) | $\eta_{ex,Plant}$ (%) |
|---|---|---|---|---|---|---|---|
| Rankine cycle (regenerative) Xu et al. (2011) | 800 | 0.75 | N.A. | 0.9 | 37.9 | 22.9 | 24.5 |
| Regenerative supercritical Rankine cycle Xu et al. (2011) | 800 | 0.75 | N.A. | 0.9 | 42.1 | 25.7 | 27.4 |
| Present work | 800 | 0.75 | N.A | 0.9 | 55.12 | 37.05 | 39.09 |
| Combined transcritical $CO_2$ cycle-ORC Chacartegui et al. (2011) | 1,000 | N.A. | 0.62 | N.A. | 43.96 | 27.14 | N.A. |
| Supercritical $CO_2$ cycle Chacartegui et al. (2011) | 1,000 | N.A. | 0.62 | N.A. | 42.48 | 26.23 | N.A. |
| Present work | 1,000 | N.A. | 0.62 | N.A. | 57.21 | 39.07 | 41.21 |

### 4.3.5 Effect of the heliostat field efficiency

Heliostat field efficiency is an important design parameter that affects plant performance. Figures 9A, B reveal that the energy, exergy, and power output of both systems increased sharply with the heliostat field efficiency. As heliostat efficiency increases, the solar energy utilization rate increases. That leads to an improvement in available energy for the power plant unit. Therefore, useful output energy increased. As the heliostat efficiency improved from 0.65 to 0.95, the energy, exergy efficiency, and power output from the proposed plant increased from 32.71% to 47.81%, from 35.03% to 51.2%, and from 16,869 kW to 24,654 kW, respectively. However, energy, exergy efficiency, and power output from the conventional SPT-HBC system increased from 24.47% to 35.76%, from 26.20% to 38.30%, and from 12,617 kW to 18,440 kW, respectively, as the heliostat field efficiency increased from 0.65 to 0.95. The performance of the system shows more improvement. Therefore, heliostat efficiency is one of the most critical parameters and must be designed carefully. Figure 9B shows the effect of heliostat field efficiency on the total cost rate of both plants. The total cost rate also increases with the heliostat field efficiency. Improving heliostat field efficiency leads to a higher temperature; consequently, the material cost of the heliostats and the receiver will increase. The total cost rate of the conventional plant (SPT-HBC) and proposed plant (SPT-HBC-ORFC) increased from $249.80/h to $256.50/h and 285.20 $/h to 302.50 $/h, respectively, as the heliostat field efficiency increased from 0.65 to 0.95.

### 4.3.6 Effect of the receiver efficiency

Figures 10A, B show how receiver efficiency affects the performance of the proposed plant. The energy efficiency, exergy efficiency, and power output of the plant also increased with the receiver efficiency. As receiver efficiency increased, the supply of solar energy to the power cycle was increased; consequently, power output also increased with the receiver efficiency, leading to efficiency improvements. It shows that thermal performance has an almost directly proportional relationship with the receiver efficiency. The energy efficiency, exergy efficiency, and power of the conventional SPT-HBC system increased from 26.66% to 29.80%, from 28.55% to 31.91%, and from 13,749 kW to 15,367 kW, respectively, when receiver efficiency increased from 0.85 to 0.95. However, the energy efficiency, exergy efficiency, and power of the proposed plant increased from 35.65% to 39.84%, from 38.18% to 42.67%, and from 18,383 kW to 20,545 kW, respectively, when the receiver efficiency increased from 0.85 to 0.95. Therefore, receiver efficiency is a critical design parameter of the solar subsection. Figure 10B also shows the variation in the total cost rate of the plants. The total cost rate increases with the receiver efficiency. Improving receiver efficiency leads to a higher temperature; consequently, the material cost of the heliostats and the receiver will increase. The total cost rate of the conventional SPT-HBC plant and the proposed plant increased from 251.10 $/h to 253 $/h and from 288.70 $/h to 293.50 $/h, respectively, as the heliostat field efficiency increased from 0.85 to 0.95.

## 4.4 Comparison with earlier studies

Irreversibilities have occurred in SPT plant components. Thus, an efficient power generation system must be implemented to improve the SPT plant's overall performance. The new SPT-based integrated system's performance is compared to previous systems published by other authors in this field. The same solar conditions are used for a true comparison, and Table 7 presents the results. According to the data, the study's combined cycle outperforms earlier comparable systems (such as the HBC-ORFC). It can be observed that the SPT-HBC-ORFC system used in this work produces superior energy efficiency than the SPT-based Rankine and $sCO_2$ systems. As such, the system offered is more efficient and has a simpler setup than other similar studies.

# 5 Conclusion

From the results and discussion section, the following conclusions are made:

- The proposed power plant's (SPT-HBC-ORFC) energy efficiency, exergy efficiency, power output, and total cost rate were 33.68%, 33.70%, 33.69%, and 15.47%, respectively, and are higher than those of a conventional SPT-HBC system at the given conditions. The improvement in thermal performance is much higher than the cost increase.
- Heliostats contribute the highest exergy destruction, accounting for 39% of the total exergy destruction.
- Parametric analysis reveals that solar subsection parameters highly affected the performance of the proposed power plant.
- Comparisons with previous studies show that the present power generation system is more efficient than other Rankine cycle and supercritical $CO_2$-based SPT systems.
- This work is limited to the peak load application due to the absence of a thermal energy storage system. Further analysis of the present work can be done in the future using a thermal energy storage system.
- Exergoeconomic and working fluid selection analysis of this system can be a topic of future research. Furthermore, instead of the ORFC system, any other low-temperature system, such as the Kalina cycle, multi-effect desalination system, etc., could be analyzed in future research.

# Data availability statement

The datasets presented in this article are not readily available because the data are confidential. Requests to access the datasets should be directed to shukla.anoophbti@gmail.com.

# Author contributions

AS: writing–original draft, visualization, validation, resources, methodology, and writing–review and editing. AKS: visualization, supervision, formal analysis, and writing–review and editing. OS: visualization, supervision, writing–review and editing, investigation, and formal analysis. MS: writing–review and editing, visualization, investigation, and formal analysis.

# Funding

The author(s) declare that no financial support was received for the research, authorship, and/or publication of this article.

# Conflict of interest

The authors declare that the research was conducted in the absence of any commercial or financial relationships that could be construed as a potential conflict of interest.

# Publisher's note

# References


Adnan, M., Zaman, M., Ullah, A., Gungor, A., Rizwan, M., and Naqvi, S. R. (2022). Thermo-economic analysis of integrated gasification combined cycle co-generation system hybridized with concentrated solar power tower. *Renew. Energy* 198, 654–666. doi:10.1016/j.renene.2022.08.088

Ahn, Y., Bae, S. J., Kim, M., Cho, S. K., Baik, S., Lee, J. I., et al. (2015). Review of supercritical $CO_2$ power cycle technology and current status of research and development. *Nucl. Eng. Technol.* 47, 647–661. doi:10.1016/j.net.2015.06.009

Alami, A. H., Olabi, A. G., Mdallal, A., Rezk, A., Radwan, A., Rahman, S. M. A., et al. (2023). Concentrating solar power (CSP) technologies: status and analysis. *Int. J. Thermofluids* 18, 100340. doi:10.1016/j.ijft.2023.100340

Bataineh, K. (2024). Hybrid fuel-assisted solar-powered stirling engine for combined cooling, heating, and power systems: a review. *Energy* 300, 131506. doi:10.1016/j.energy.2024.131506

Behar, O., Sbarbaro, D., and Moran, L. (2021). Which is the most competitive solar power technology for integration into the existing copper mining plants: photovoltaic (PV), Concentrating Solar Power (CSP), or hybrid PV-CSP? *J. Clean. Prod.* 287, 125455. doi:10.1016/j.jclepro.2020.125455

Bejan, A., Tsatsaronis, G., and Moran, M. (1996). *Thermal design and optimization*. NewYork: John Wiley and Sons Inc.

Chacartegui, R., Muñoz de Escalona, J. M., Sánchez, D., Monje, B., and Sánchez, T. (2011). Alternative cycles based on carbon dioxide for central receiver solar power plants. *Appl. Therm. Eng.* 31, 872–879. doi:10.1016/j.applthermaleng.2010.11.008

Dunham, M. T., and Iverson, B. D. (2014). High-efficiency thermodynamic power cycles for concentrated solar power systems. *Renew. Sustain Energy Rev.* 30, 758–770. doi:10.1016/j.rser.2013.11.010

Huang, Y., Jiang, P., and Zhu, Y. (2022). Analysis of a novel combined cooling and power system by integrating of supercritical $CO_2$ Brayton cycle and transcritical ejector refrigeration cycle. *Energy Convers. Manag.* 269, 116081. doi:10.1016/j.enconman.2022.116081

Khan, Y., Apparao, D., Gawande, S., Singh, N., Bisht, Y. S., and Singh, P. (2024b). Performance assessment and working fluid selection of the novel combined helium Brayton cycle and organic rankine cycle based on solar power tower for sustainable generation. *Trans. Mech. Eng.* 48, 1901–1916. doi:10.1007/s40997-023-00745-8

Khan, Y., and Mishra, R. S. (2021). Performance evaluation of solar-based combined pre-compression supercritical $CO_2$ cycle and organic Rankine cycle. *Int. J. Green Energy* 18 (2), 172–186. doi:10.1080/15435075.2020.1847115

Khan, Y., and Mishra, R. S. (2023a). Performance investigation of the solar power tower driven combined cascade supercritical $CO_2$ cycle and organic Rankine cycle using HFO fluids. *Aust. J. Mech. Eng.* 21 (5), 1714–1728. doi:10.1080/14484846.2022.2030087

Khan, Y., and Mishra, R. S. (2023b). Performance analysis of a solar based novel trigeneration system using cascaded vapor absorption-compression refrigeration system. *Int. J. Refrig.* 155, 207–218. doi:10.1016/j.ijrefrig.2023.08.014

Khan, Y., Raman, R., Rashidi, M. M., Said, Z., Caliskan, H., and Hoang, A. T. (2024a). Thermodynamic and exergoenvironmental assessments of solar-assisted combined power cycle using eco-friendly fluids. *J. Therm. Analysis Calorim.* 149, 1125–1139. doi:10.1007/s10973-023-12760-7

Khan, Y., Singh, D., Caliskan, H., and Hong, H. (2023). Exergoeconomic and thermodynamic analyses of solar power tower based novel combined helium Brayton cycle-transcritical $CO_2$ cycle for carbon free power generation. *Glob. Challenges* 7, 2300191. doi:10.1002/gch2.202300191

Khan, Y., and Singh, P. K. (2024). Thermo-economic and environmental assessment of a novel SOFC based hybrid energy generation system for combined cooling heating and power generation. *J. Energy Resour. Technol.*, 1–25. doi:10.1115/1.4066110

Klein, S. A. (2018). "Engineering equation solver (EES)," in *Academic commercial V7.714. F-chart software*. Available at: www.fChart.com.

Lee, Ho Y., and Sang, H. P. (2016). Kyoung Hoon Kim Comparative analysis of thermodynamic performance and optimization of organic flash cycle (OFC) and organic Rankine cycle (ORC). *Appl. Therm. Eng.* 100, 680–690. doi:10.1016/j.applthermaleng.2016.01.158

Ma, Y., Morozyuk, T., Liu, M., Yan, J., and Liu, J. (2019). Optimal integration of recompression supercritical $CO_2$ Brayton cycle with main compression intercooling in solar power tower system based on exergoeconomic approach. *Appl. Energy* 242, 1134–1154. doi:10.1016/j.apenergy.2019.03.155

Mahmoud, M., Naher, S., Ramadan, M., Abdelkareem, M. A., Jaber, H., and Olabi, A. G. (2023). Investigation of a ground-cooled organic Rankine cycle for waste heat recovery. *Int. J. Thermofluids* 18, 100348. doi:10.1016/j.ijft.2023.100348

Mehrpooya, M., Ashouri, M., and Mohammadi, A. (2017). Thermoeconomic analysis and optimization of a regenerative two-stage organic Rankine cycle coupled with liquefied natural gas and solar energy. *Energy126* 126, 899–914. doi:10.1016/j.energy.2017.03.064

Nasouri, M., and Delgarm, N. (2023). Numerical modeming, energy–exergy analyses, and multi-objective programming of the solar-assisted heat pump system using genetic algorithm coupled with the multi-criteria decision analysis. *Arabian J. Sci. Eng.* 48, 3537–3557. doi:10.1007/s13369-022-07151-3

Nondy, J., and Gogoi, T. K. (2021). Exergoeconomic investigation and multi-objective optimization of different ORC configurations for waste heat recovery: a comparative study. *Energy Convers. Manag.* 245, 114593. doi:10.1016/j.enconman.2021.114593

Pan, M., Chen, X., and Li, X. (2022). Multi-objective analysis and optimization of cascade supercritical $CO_2$ cycle and organic Rankine cycle systems for waste-to-energy power plant. *Appl. Therm. Eng.* 214, 118882. doi:10.1016/j.applthermaleng.2022.118882

Qin, L., Xie, G., Ma, Y., and Li, S. (2023). Thermodynamic analysis and multi-objective optimization of a waste heat recovery system with a combined supercritical/transcritical $CO_2$ cycle. *Energy* 265, 126332. doi:10.1016/j.energy.2022.126332

Roux, D. L., Olivès, R., and Neveu, P. (2024). Multi-objective optimisation of a thermocline thermal energy storage integrated in a concentrated solar power plant. *Energy* 300, 131548. doi:10.1016/j.energy.2024.131548

Tang, J., Li, Q., Wang, S., and Yu, H. (2023). Thermo-economic optimization and comparative analysis of different organic flash cycles for the supercritical $CO_2$ recompression Brayton cycle waste heat recovery. *Energy* 278 (2023), 128002. doi:10.1016/j.energy.2023.128002

Wang, Z., Chen, H., Xia, R., Han, F., Ji, Y., and Cai, W. (2022). Energy, exergy and economy (3E) investigation of a SOFC-GT-ORC waste heat recovery system for green power ships. *Therm. Sci. Eng. Prog.* 32, 101342. doi:10.1016/j.tsep.2022.101342

Wu, C., and Wang, S.-sen (2018). Jun Li. Exergoeconomic analysis and optimization of a combined supercritical carbon dioxide recompression Brayton/organic flash cycle for nuclear power plants. *Energy Convers. Manag.* 171, 936–952. doi:10.1016/j.enconman.2018.06.041

Xu, C., Wang, Z., Li, X., and Sun, F. (2011). Energy and exergy analysis of solar power tower plants. *Appl. Therm. Eng.* 31, 3904–3913. doi:10.1016/j.applthermaleng.2011.07.038

Zare, V., Mahmoudi, S. M. S., and Yari, M. (2015). On the exergoeconomic assessment of employing Kalina cycle for GT-MHR waste heat utilization. *Energy Convers. Manag.* 90, 364–374. doi:10.1016/j.enconman.2014.11.039

Zendehnam, A., and Pourfayaz, F. (2024). Advanced exergy and advanced exergoeconomic analyses of the partial heating supercritical $CO_2$ power cycle for waste heat recovery. *J. Therm. Analysis Calorim.* 149, 3397–3414. doi:10.1007/s10973-024-12913-2

Zhou, J., Ali, M. A., Zeki, F. M., and Dhahad, H. A. (2023). Thermoeconomic investigation and multi-objective optimization of a novel efficient solar tower power plant based on supercritical Brayton cycle with inlet cooling. *Therm. Sci. Eng. Prog.* 39, 101679. doi:10.1016/j.tsep.2023.101679

Zhu, H., Xie, G., Yuan, H., and Nizetic, S. (2022). Thermodynamic assessment of combined supercritical $CO_2$ cycle power systems with organic Rankine cycle or Kalina cycle. *Sustain. Energy Technol. Assessments* 52, 102166. doi:10.1016/j.seta.2022.102166

# Nomenclature

| | |
|---|---|
| $\dot{C}$ | cost rate ($/h) |
| $\dot{Ed}$ | exergy destruction rate (kW) |
| $\dot{Ex}$ | rate of exergy (kW) |
| $N_{hel}$ | number of heliostats (–) |
| $\dot{Q}$ | heat rate (kW) |
| $\dot{W}$ | power output (kW) |
| $\dot{Z}$ | capital cost rate ($/h) |
| $\dot{m}$ | mass flow rate (kg/s) |
| $A$ | area ($m^2$) |
| $h$ | specific enthalpy (kJ/kg) |
| $s$ | specific entropy (kJ/kg°C) |
| $T$ | temperature (K) |

## Abbreviations

| | |
|---|---|
| *COND* | condenser |
| *DNI* | direct normal irradiation |
| *FS* | flash separator |
| *HBC* | helium Brayton cycle |
| *HRVG* | heat recovery vapor generator |
| *HTF* | heat transfer fluid |
| *IHE* | intermediate heat exchanger |
| *IHX* | internal heat exchanger |
| *ORC* | organic rankine cycle |
| *PC* | precooler |
| *PR* | compressor pressure ratio |
| *RORC* | recuperative-regenerative ORC |
| *sCO$_2$* | supercritical $CO_2$ |
| *SPT* | solar power tower |
| *T1* | Turbine-1 |
| *T2* | Turbine-2 |
| *tCO$_2$* | transcritical carbon dioxide |

## Subscripts

| | |
|---|---|
| *0* | dead condition |
| *of* | organic fluid (R290) |
| *e* | exit |
| *ex* | exergy |
| **en** | energy |
| *hel* | heliostat |
| *rec* | receiver |
| *i* | inlet, $i^{th}$ state |
| *j* | $j^{th}$ component |
| *comp* | compressor |
| *comb* | combined cycle |

## Greek letters

| | |
|---|---|
| $\eta$ | efficiency |
| $\varepsilon$ | effectiveness |